Reentrant miscibility in two-dimensional symmetrical mixtures

S. Materniak, A. Patrykiejew,* and W. Rżysko
Department for the Modelling of Physico-Chemical Processes, Faculty of Chemistry, MCS University, 20031 Lublin, Poland
(Received 18 March 2013; published 13 June 2013)

The Monte Carlo simulation method in the grand canonical ensemble is used to study the phase behavior of two-dimensional symmetrical binary mixtures of Lennard-Jones particles with negative nonadditivity and the weaker interaction between the pairs of unlike than between the pairs of like particles. We have determined the evolution of the phase diagram topology when the parameters describing the interaction between unlike particles vary. It has been found that such systems may exhibit reentrant miscibility in the liquid and the solid phases.

DOI: 10.1103/PhysRevE.87.062306 PACS number(s): 64.75.−g, 61.20.Ja, 64.70.Ja, 64.70.K−

I. INTRODUCTION

Demixing transitions and miscibility gaps are very common in multicomponent systems. Demixing transitions may be driven by cohesive forces or by entropy [1]. The first situation usually occurs in simple systems containing components of comparable size, while entropy-driven demixing occurs when the components considerably differ in size. The simplest model system exhibiting entropy-driven phase separation is a binary nonadditive hard sphere mixture [2–4]. Here, we are rather interested in the systems that undergo demixing transitions due to interplay of entropic and energetic effects. Therefore, we consider the a simple model of nonadditive symmetrical mixture involving repulsive and attractive interactions. The pure components exhibit the existence of gas, liquid, and solid phases, so that the mixture may also form such phases.

A model of symmetrical binary mixture (SBM) assumes that interactions between like particles (*A*-*A* and *B*-*B*) are the same, while the interaction between unlike particles (*A*-*B*) is different [1]. Uniform, three- and two-dimensional SBMs have been studied using different theoretical approaches and computer simulation methods [5–25]. It has been demonstrated that this simple model exhibits surprisingly rich phase behavior and leads to different phase diagram topologies [10,25], primarily depending on the interaction between unlike particles. In particular, the liquid phase has been found to phase separate when the interaction between the unlike pairs is weaker than the interaction between the like pairs. Usually, the demixing transition is of first order at low temperatures, when the demixed liquid coexists with a dilute vapor, and continuous at high temperatures. The onset of continuous phase separation may occur at the tricritical point (T_{trc}), which replaces the gas-liquid critical point, or at the critical end point (T_{cep}) at the liquid side of the gas-liquid coexistence below the gas-liquid critical point. At the temperatures above T_{trc} or T_{cep}, the demixing transition occurs along the line of consolute points $T_\lambda(\rho)$ (ρ being the total density of the fluid), i.e., along the so-called λ-line.

It has recently been shown [24,25] that in the case of two-dimensional SBMs of Lennard-Jones particles, the slope of λ line [$\delta_{\lambda,\rho} = dT_\lambda(\rho)/d\rho$] strongly depends on the geometrical nonadditivity $s = 2\sigma_{AB}/(\sigma_{AA} + \sigma_{BB}) - 1$ and leads to quite complex phase behavior when one takes into account the liquid-solid transition. In particular, it has been demonstrated that when s is considerably larger than zero (e.g., $s = 0.24$), the slope $\delta_{\lambda,\rho}$ is larger than the slope of the freezing line, i.e., the density derivative of the liquid-solid coexistence temperature at the liquid side (δ_f). In such cases, the λ line does not meet the liquid-solid coexistence and the solid is demixed up to high temperatures. On the other hand, it has been found that for $s = 0$, the slope $\delta_{\lambda,\rho}$ is lower than δ_f and the λ line, which starts at the tricritical point or at the lower critical end point ($T_{\mathrm{l,cep}}$), meets the liquid-solid coexistence at the upper critical end point ($T_{\mathrm{u,cep}}$), leading to the phase diagram as that depicted in Fig. 4 of Ref. [25]. In such cases, the solid phase is demixed at low temperatures and mixed at high temperatures. The demixing transition in the solid begins at the critical end point located at the solid side of the liquid-solid coexistence ($T_{\mathrm{cep,sol}}$) at the temperature above the upper critical end point of the liquid demixing transition. These different scenarios are closely related to the packing effects and the changes of the liquid phase structure when the parameter s changes.

Another interesting problem involves the possibility of closed-loop immiscibility in mixtures with spherical interactions. It has been commonly accepted for a long time that this sort of behavior results from the presence of strong orientational interactions [26–28]. Some time ago, Lopes [29] performed computer simulation that demonstrated closed-loop immiscibility in the mixtures with isotropic interactions, if the range of interaction between unlike particles is shorter than the interaction between like species. Then, Almarza *et al.* [30] showed that the SBMs with the square well pair potential and negative nonadditivity ($s < 0$) also exhibited a closed-loop immiscibility, so that the phase diagram of class VI [31], not obtainable within the framework of van der Waals theory, appeared. Their results, based on the perturbation theory of Barker and Henderson [32] and Monte Carlo simulation in the semigrand canonical ensemble [33], have demonstrated that reentrant miscibility occurs over a certain range of $s < 0$ and again only when the *AB* attractive interaction (ε_{AB}) is of shorter range and stronger than the attraction between the pairs of like particles ($\varepsilon_{AA} = \varepsilon_{BB}$).

In this paper, we show that in the case of SBMs with the Lennard-Jones pair potential the reentrant miscibility also occurs in the systems with negative additivity, but only when the interaction between unlike pairs is weaker than the interaction between like pairs.

*andrzej.patrykiejew@gmail.com

The paper is organized as follows. In the next section, we define our model and briefly discuss the simulation methods. Then, in Sec. III we present and discuss our results. Finally, we summarize our findings in Sec. IV.

II. THE MODEL AND MONTE CARLO METHODS

We consider strictly two-dimensional symmetrical mixtures consisting of atoms A and B, which interact via the truncated (12,6) Lennard-Jones potential

$$u_{ij}(r) = \begin{cases} 4\varepsilon_{ij}[(\sigma_{ij}/r)^{12} - (\sigma_{ij}/r)^{6}] & r \leqslant r_{\max} \\ 0 & r > r_{\max}, \end{cases} \quad (1)$$

where r is the distance between a pair of atoms, i and j mark the species A and B, and the potential is cut at the distance $r_{\max} = 3.0\sigma_{ij}$. In the case of symmetrical mixtures, the potential parameters describing the interaction between like particles are the same; i.e., $\sigma_{AA} = \sigma_{BB} = \sigma$ and $\varepsilon_{AA} = \varepsilon_{BB} = \varepsilon$. The corresponding potential parameters for a pair of unlike atoms are given by

$$\sigma_{AB} = (s+1)\sigma \quad \text{and} \quad \varepsilon_{AB} = e\varepsilon, \quad (2)$$

and σ and ε are taken as the units of length and energy, respectively. Thus, the temperature is given in the units of ε/k and the chemical potentials of both species μ_i $(i = A, B)$ and the other energy-like quantities are given in the units of ε.

The model has been studied using Monte Carlo simulation method in the grand canonical ensemble [34–36] under the condition of equality of the chemical potentials of both species $(\mu_A = \mu_B = \mu)$. Calculations have been carried out using the simulation cells of the size $L \times L$, with $L = 20$ and 30 and with the standard periodic boundary conditions.

The quantities recorded included the average numbers of particles A (N_A) and B (N_B), the order parameter

$$m = (N_A - N_B)/(N_A + N_B), \quad (3)$$

the average potential energy $\langle e \rangle$, and the radial distribution functions, $g_{i-j}(r)$, for $i - j = A - A$, $A - B$, and $B - B$.

We have also calculated the probability distributions of the order parameter $[p(m)]$ of the densities of individual components $p(\rho_A)$ and $p(\rho_B)$ as well as the probability distribution of the total density $[p(\rho)]$. Calculations of these distribution functions have been carried out using hyperparallel tempering method [36].

III. RESULTS AND DISCUSSION

The calculations have been carried out for several systems characterized by the values of the parameter s ranging between -0.26 and 0.0 and with the parameter e ranging between 0.5 and 0.8. In all cases, the potential well for like pairs is deeper and, apart from the system with $s = 0$, of longer range than for unlike pairs.

We shall demonstrate that the shorter range of the interaction between unlike particles as compared to the like particles considerably affects the phase behavior and may lead to the reentrant miscibility in the liquid phase. It will also be demonstrated that different solid phases appear in the systems considered here.

To begin with, we consider a series of systems characterized by the fixed value of the parameter $e = 0.8$. From the results of our earlier study [25], it follows that in the case of $s = 0$ the liquid does not phase separate and demixing transition occurs only in the solid phase. The onset of the demixing transition is located at the temperature below the triple point $T_{\mathrm{tr,vl}_m s_{m,h}} \approx 0.373$. At the triple point, the vapor (v) coexists with a mixed liquid (l_m) and with also mixed solid of hexagonal symmetry $(s_{m,h})$. The same qualitative results have been obtained for the system with $s = -0.05$. The phase diagram topology for these systems is similar to one shown in part g of Fig. 9 of Ref. [25].

Upon the decrease of s to -0.1, the tendency toward demixing appears to increase and we have found that the demixing transition occurs at the temperatures above the triple point, i.e., already in the liquid phase. Figure 1 shows the phase diagram obtained for this system. One notes that the λ line originates at the lower critical end point at the liquid side of the vapor-liquid coexistence at $T_{\mathrm{l,cep}} \approx 0.388$ and ends at the upper critical end point at the liquid side of the liquid-solid coexistence at $T_{\mathrm{u,cep}} \approx 0.382$. The locations of the demixing transition have been estimated using the distribution functions of the order parameter m $[p(m)]$ and of the system density ρ $[p(\rho)]$ obtained for the systems of different size of the simulation cell. The examples of these distributions are shown in the inset to Fig. 1(b). It should be emphasized

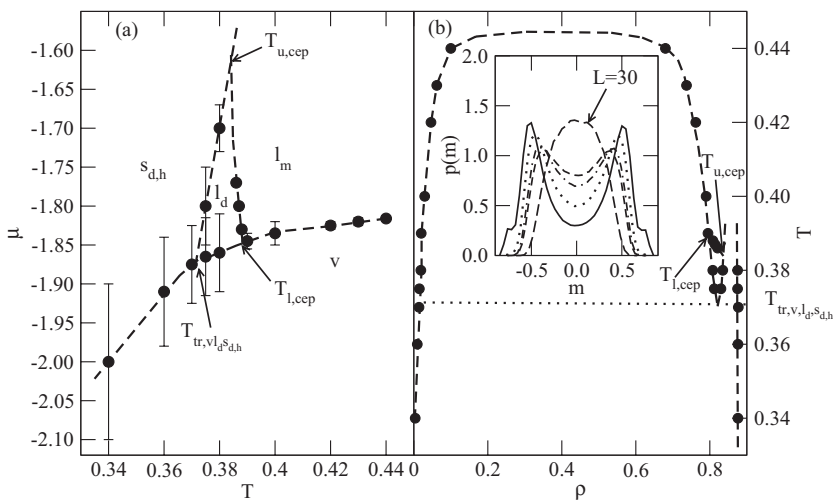

FIG. 1. The phase diagram for the system with $e = 0.8$ and $s = -0.1$. Part a (b) shows the $T - \mu$ $(T - \rho)$ projection. The inset to part b shows the probability distributions of the order parameter m obtained for $\mu = -1.77$ and at different temperatures equal to (0.38, solid line; 0.384, dotted line; 0.388, dash-dotted line; and 0.39, short-dashed lines) using the simulation cell with $L = 20$. The long-dashed line represents the distribution obtained at $T = 0.39$ and $L = 30$.

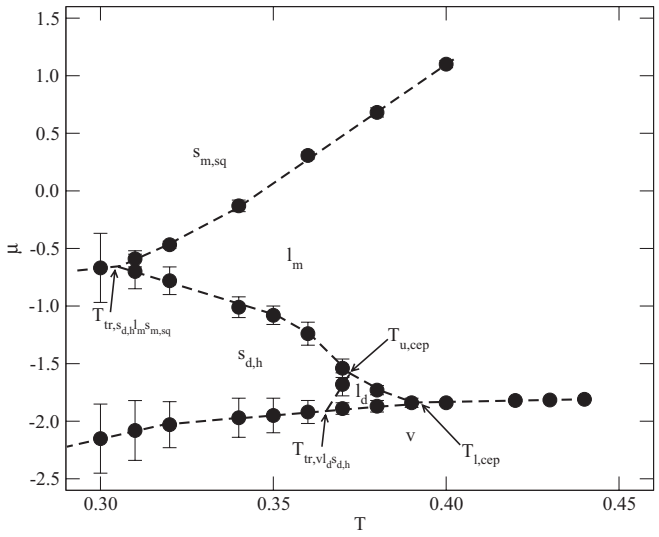

FIG. 2. The $T - \mu$ projection of the phase diagram for the system with $e = 0.8$ and $s = -0.13$.

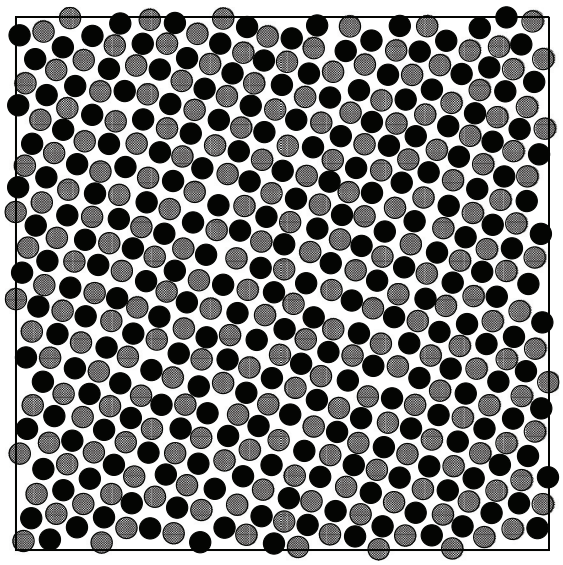

FIG. 3. The snapshot recorded for the system with $e = 0.8$ and $s = -0.13$ at $T = 0.2$ and $\mu = 0.0$.

that the order parameter distributions obtained for rather small simulation cell with $L = 20$ show very large finite-size effects being responsible for the bimodal distributions $p(m)$ even at the temperatures above the demixing transition. When a larger simulation cell with $L = 30$ is used, the distribution $p(m)$ recorded above the temperature of demixing transition does not show the bimodal shape as the inset to Fig. 1(b) illustrates. The distribution recorded at $T = 0.38$ also shows small contributions due to demixed solid. This is caused by the proximity of the thermodynamic state, determined by T and μ, to the liquid-solid coexistence.

An interesting feature of this system is that the λ line has a negative slope with respect to the chemical potential $\delta_{\lambda,\mu} = dT_\lambda(\mu)/d\mu$. Therefore, the lower critical end point occurs at the temperature (slightly) higher than the upper critical end point. Of course, also the slope $\delta_{\lambda,\rho}$ is negative. In consequence, the compression of a demixed liquid leads to reentrant mixing.

The solid phase has been found to be demixed at the temperatures below the upper critical end point and mixed at higher temperatures. We have not performed calculations suitable to locate the transition temperature. A direct examination of configurations and the calculations of radial distribution functions have shown that both demixed and mixed solid phases have a hexagonal symmetry, as in the case of $s = 0$.

In the case of lower s equal to -0.13 (and also when $s = -0.15$), the phase diagram exhibits new features (see Fig. 2). The λ line starts at the lower critical end point at the liquid side of the vapor-liquid coexistence and also has negative slopes $\delta_{\lambda,\rho}$ and $\delta_{\lambda,\mu}$, and it ends at the upper critical end point. At this point, a demixed solid of hexagonal symmetry coexists with two critical (mixed and demixed) liquid phases. It appears that the mixed liquid remains stable at the temperatures below the upper critical end point, down to the triple-point temperature, $T_{\mathrm{tr},s_{d,h}l_m s_{m,\mathrm{sq}}}$, at which the two demixed solid and mixed liquid coexist with a mixed solid phase. At the temperatures above $T_{\mathrm{tr}},s_{d,h}l_m s_{m,\mathrm{sq}}$, the mixed liquid freezes into a mixed solid at sufficiently high density. Unlike in the system with $s = -0.1$, the mixed solid has a different structure and shows a quite well developed square symmetry. In this phase, each A (B) particle has four B (A) nearest neighbors (see Fig. 3). At the temperatures below $T_{\mathrm{tr},s_{d,h}l_m s_{m,\mathrm{sq}}}$, a first-order transition between the two solid phases takes place. Although it is not straightforward to find the ground-state properties of the system considered here, we have estimated the locations of the gas-demixed solid and demixed solid-mixed solid transition points and found that the former occurs at μ of about -3.35, while the latter is located at the considerably higher chemical potential of about -0.85. The ground-state calculation has been performed assuming that the demixed solid is a perfectly ordered hexagonal array of only one type of particle and that the mixed solid is a perfect square lattice in which each A (B) particle has only B (A) nearest neighbors. We have constructed appropriate configurations and then minimized the energy with respect to nearest-neighbor distance. Of course, at nonzero temperatures, the demixed solid is bound to contain some small amount of the second component, just the same as it occurs in the demixed liquid phase.

The above presented results suggest that for s between -0.1 and -0.13 there should be a crossover from the region in which the mixed solid has a hexagonal symmetry (large s regime) to the region favoring square ordering in the mixed solid phase (small s regime). At this point, it is appropriate to recall that the Monte Carlo studies of Vlot *et al.* [20,37,38], performed in the NPT ensemble, have demonstrated that at sufficiently low temperatures the two-dimensional SBM with $s = -0.13$ and $e = 1.0$ forms a solid of square symmetry and its three-dimensional counterpart forms a body-centered cubic crystal.

The system with a lower value of $s = -0.16$ has shown that demixing transition in the liquid occurs over very narrow region of T, between about 0.363 and 0.37 (see Fig. 4). The probability distributions of the order parameter m recorded at $T = 0.365$ and for the chemical potentials slightly above the vapor-liquid coexistence have clearly demonstrated the presence of the transition between the demixed and mixed

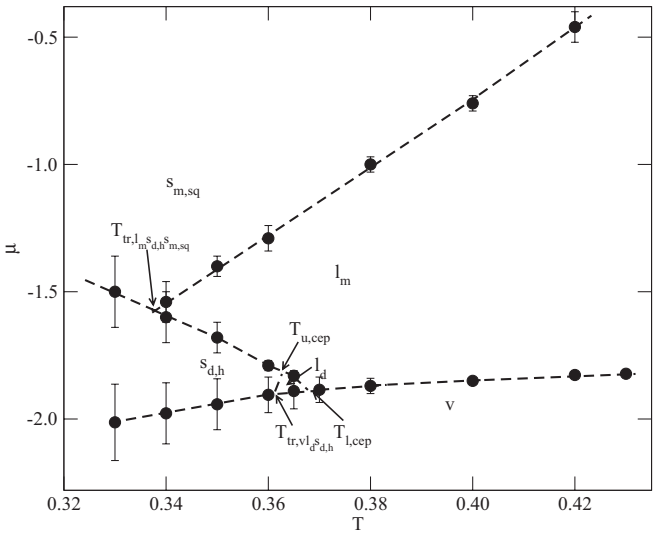

FIG. 4. The $T-\mu$ projection of the phase diagram for the system with $e=0.8$ and $s=-0.16$.

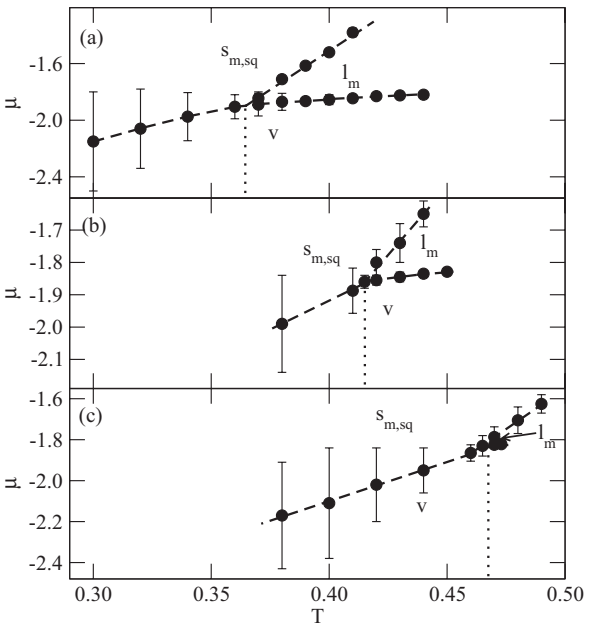

FIG. 5. The $T-\mu$ projections of the phase diagrams for the systems with $e=0.8$ and different values of $s=-0.18$ (part a), -0.20 (part b), and -0.22 (part c).

liquid phases upon the increase of the chemical potential and, hence, of the density. On the other hand, the distributions recorded at $T=0.37$ have shown that the vapor condenses into an already mixed liquid.

Comparing the phase diagrams depicted in Figs. 2 and 4, one readily notes that at sufficiently low temperatures, also the region of chemical potential over which the demixed solid is stable becomes narrower when s becomes smaller. This suggests that for still lower values of s we should not observe the demixed liquid and solid phases at all. Indeed, the calculations performed for the systems with $s=-0.18$, -0.2, and -0.22 have shown that only mixed liquid and solid of square symmetry appear. The phase diagrams for these three systems are given in Fig. 5. Two important effects should be noted. The triple point temperature shows a rather sharp increase upon the lowering of s. The critical temperature increases also, but not so sharply. The reason is that the stability of a solid phase of square symmetry increases due to a better fit of AB pairs and the decrease of the second nearest neighbors, which are of the same kind and exhibit stronger attraction. Therefore, the potential energy becomes lower while the entropic effects are not much affected by rather small changes in interatomic distances. Similarly, the potential energy contribution in the liquid becomes more and more important when the parameter s is lower. The radial distribution functions have demonstrated that the mixed liquid is locally ordered. The upper panel of Fig. 6 presents a comparison of the radial distribution functions $g_{A-A}(r)$ and $g_{A-B}(r)$ obtained for the system with $s=-0.2$ at the temperature $T=0.42$, i.e., above the triple point and for two values of the chemical potential in the regions of stability of a liquid ($\mu=-1.8$) and of a solid ($\mu=-1.7$) phase. The first peak at $g_{A-A}(r)$ corresponds to the second nearest neighbors. In the perfectly ordered solid, the maximum of this peak should occur at $r=\sqrt{2}r_{NN}$, where r_{NN} is the first nearest-neighbor distance, specified by the location of the first maximum at $g_{A-B}(r)$. Of course, at the temperature above the triple point, the solid is not perfectly ordered and slightly expanded, so that this peak is broader and its maximum is located at larger distance than $\sqrt{2}r_{NN}$. The lower panel of Fig. 6 shows the radial distribution functions $g_{A-A}(r)$ and $g_{A-B}(r)$ recorded at $T=0.32$. The first maximum of $g_{A-B}(r)$ is located at $r_{NN}\approx 0.86$, while the first maximum of g_{A-A} occurs for $r=1.218$, very close to the value of 1.216 predicted for a perfectly ordered mixed solid.

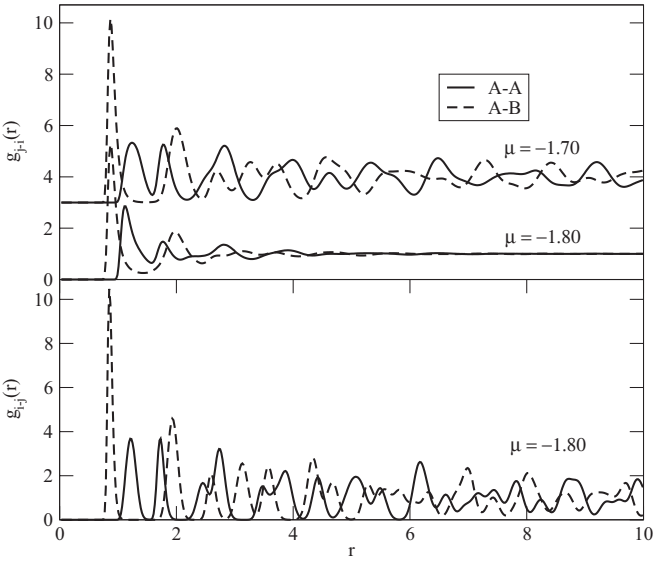

FIG. 6. The upper panel shows the radial distribution functions $g_{A-A}(r)$ and $g_{A-B}(r)$ for the liquid ($\mu=-1.80$) and the solid ($\mu=-1.70$) obtained for the system with $e=0.8$ and $s=-0.2$ at $T=0.42$. Note that the radial distribution functions of the solid are shifted upwards by three units. The lower panel gives $g_{A-A}(r)$ and $g_{A-B}(r)$ for the solid phase at $T=0.32$.

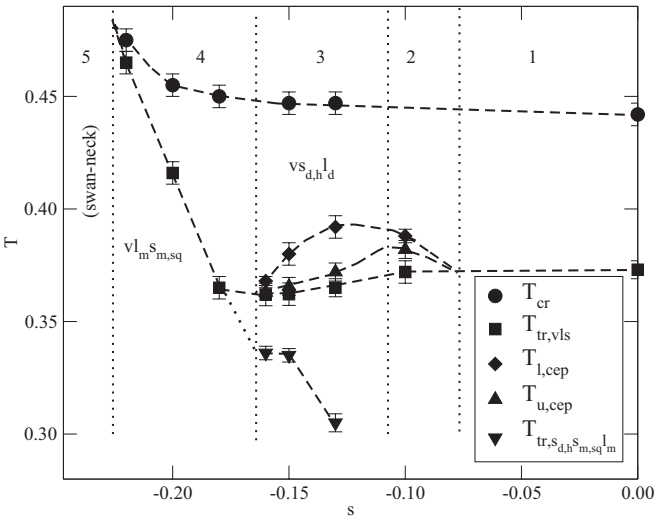

FIG. 7. The changes in the phase diagram topology with s for the systems with $e = 0.80$.

The summary of our findings for the above discussed systems with $e = 0.8$ is given in Fig. 7, which presents the changes of the temperatures at critical points, tricritical points, triple points, and critical end points versus the parameter s. Our results have allowed the five different regions of s to be singled out. In each of them, the phase diagrams have different topology.

In the region 1, the liquid does not undergo demixing transition at all, and only the solid exhibits a continuous transition between the low-temperature demixed and high-temperature mixed phases. The onset of this transition occurs in the critical end point, located at the solid side of the liquid-solid coexistence. When s decreases from 0 to about

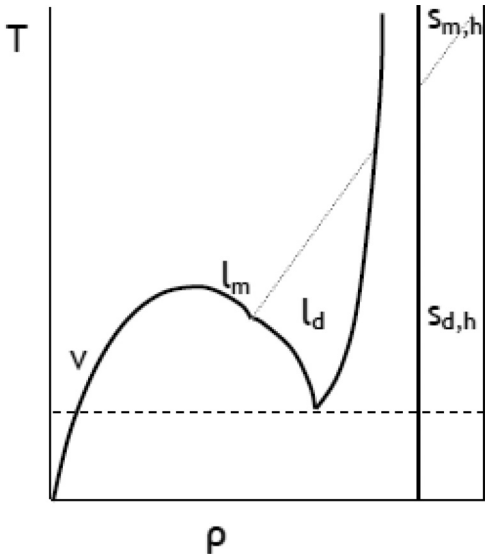

FIG. 8. Schematic representation of the phase diagram [$T - \mu$ ($T - \rho$) projection] for the systems characterized by $e = 0.8$ and the parameter s between 0 and -0.05. The regions labeled with v, l_m, l_d, $s_{d,h}$, and $s_{m,h}$ correspond to the vapor, mixed liquid, demixed liquid, demixed solid of hexagonal symmetry, and mixed solid of hexagonal symmetry, respectively.

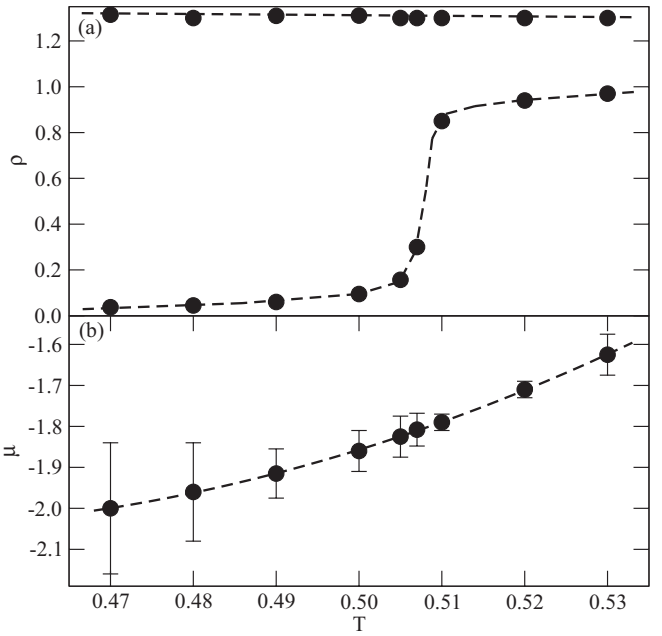

FIG. 9. The $T - \mu$ (part a) and $T - \rho$ (part b) projections of the phase diagram for the system with $e = 0.8$ and $s = -0.24$.

-0.075, the critical end-point temperature gradually increases. In this region, the phase diagram topology is like that shown in Fig. 8.

When s drops below about -0.075, the situation changes and we enter region 2, in which the liquid undergoes a demixing transition. This transition starts at the lower critical end point and ends at the upper critical end point. Our results obtained for $e = 0.8$ have demonstrated that the slope $\delta_{\lambda,\mu}$ of the λ line is negative, and hence $T_{\mathrm{l,cep}} > T_{\mathrm{u,cep}}$. In this region, the two solid phases (mixed and demixed) are hexagonally ordered and the phase diagrams are similar to the one shown in Fig. 8.

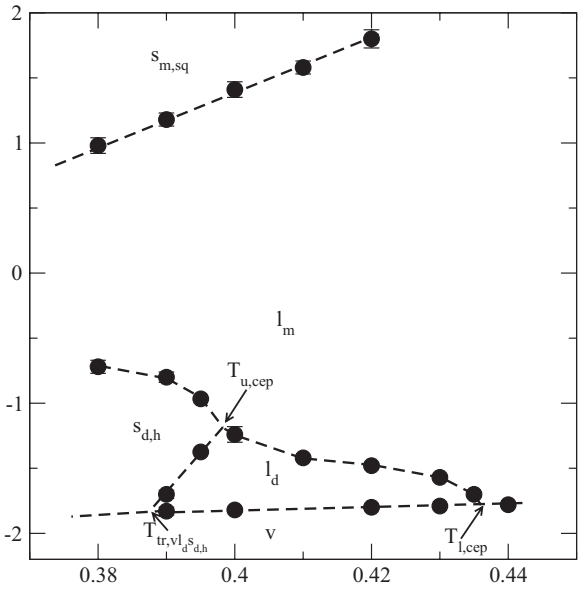

FIG. 10. The $T - \mu$ projection of the phase diagram for the system with $s = -0.13$ and $e = 0.75$.

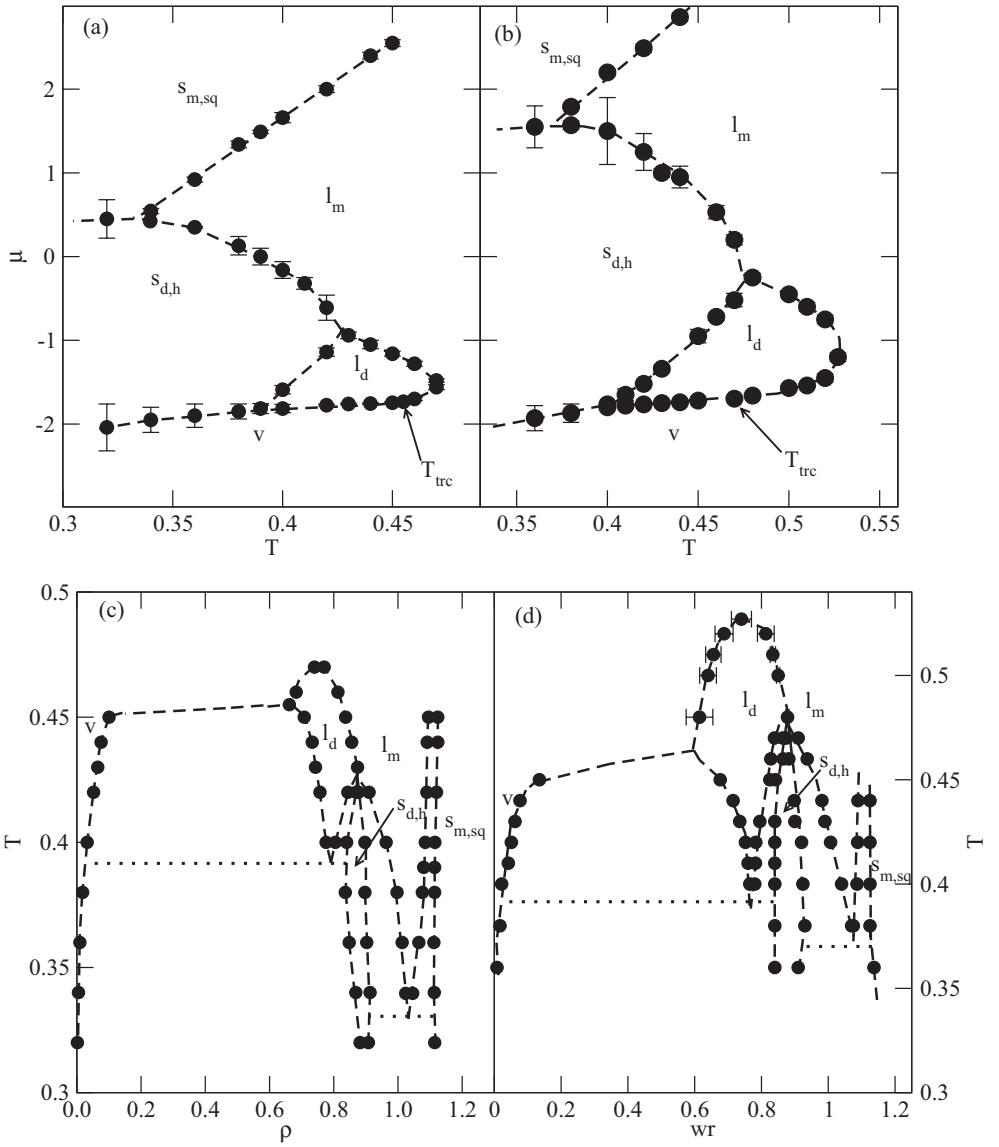

FIG. 11. Parts a and b (c and d) show the $T-\mu$ ($T-\rho$) projections of the phase diagrams for the systems with $s=-0.13$ and two different values of e equal to 0.7 (parts a and c) and 0.6 (parts b and d).

Upon the decrease of s below about -0.11, the behavior changes and one enters region 3. Similarly as in region 2, the liquid also undergoes demixing transition, which starts at the lower critical end point and ends at the upper critical end point. The difference between regions 2 and 3 is that in the former the mixed solid also has a hexagonal symmetry, while in the latter it is square ordered. In this region, the phase diagrams like those shown in Figs. 2 and 4 are found. It should be noted that the triple-point temperature, at which the two solid phases coexist with a mixed liquid, decreases when the parameter s increases, and one expects that it drops down to zero when s reaches the value at the boundary between regions 2 and 3.

When s becomes lower that about -0.165, we enter region 4, in which only mixed liquid and solid phases are present. In this region, the phase diagrams like those given in Fig. 5 appear. The critical temperature of the vapor-liquid condensation shows a rather large increase with the lowering of s. Also, the triple-point temperature increases even more sharply, when parameter s decreases.

The data given in Fig. 7 shows that for the value of s equal to about -0.227, the critical and triple points should merge and we enter region 5, in which one expects to find a swan-neck type of phase diagram. Indeed, the calculations carried out for the system with $s=-0.24$ have confirmed that prediction very well and have led to the phase diagram given in Fig. 9.

Now, we turn to the presentation of results for the systems with smaller values of the parameters e, i.e., for the systems exhibiting higher tendency toward demixing, and consider the behavior of SBMs with $s<0$. The results for the systems with $s=0$, given in Ref. [25], have demonstrated that for e greater than about 0.76, the liquid does not phase separate at all while the solid is demixed at low temperatures and undergoes a transition to a mixed phase at sufficiently high temperatures. Both demixed and mixed solid phases have

hexagonal symmetry as expected for the system without nonadditivity effects of the parameters σ_{ij}. The continuous transition between the demixed and mixed solid phases occurs along the line of consolute points and starts at the critical end point, located at the solid side of the fluid-solid coexistence. It has been verified that this transition belongs to the universality class of the Ising model, just the same as the demixing transition in the liquid [10,25]. Of course, the critical end point travels along the coexistence toward higher temperatures when the parameter e becomes lower. As soon as e drops below 0.76, the liquid also exhibits a demixing transition over a certain range of temperatures either between the lower and upper critical end points (when e is greater than about 0.66) or between the tricritical point and the upper critical end point ($e < 0.66$). The schematic representation of the phase diagrams for these systems has been shown in Fig. 9 of Ref. [25].

In the systems with s lower than zero and $e < 0.8$, the tendency toward demixing also increases. Thus, the lower critical end point, being the onset of the demixing transition in the liquid, moves toward higher temperatures. Besides, the slope of the λ line is expected to decrease when s becomes lower, as in the previously discussed case of $e = 0.8$ (cf. Figs. 1 and 2). It has already been shown that for $s \leqslant -0.1$ and $e = 0.8$, the slope $\delta_{\lambda,\mu}$ is negative and leads to the transition from a demixed to a mixed liquid when density increases. For lower values of e, the temperature range over which the reentrant miscibility occurs becomes wider. Figure 10 shows the phase diagram for the system with $e = 0.75$ and $s = -0.13$, which demonstrates that reentrant miscibility occurs over a considerably wider temperature range than observed in the case of $e = 0.8$ (cf. Fig. 2). This scenario holds as long as the λ line begins in the lower critical end point at the liquid side of the vapor liquid coexistence below the critical point. When, however, the parameter e becomes low enough, the λ line begins rather in the tricritical point than in the critical end point. In such cases, the λ line forms a loop and reentrant miscibility is observed also above the tricritical point. In Fig. 11, we have presented two phase diagrams obtained for the systems with $s = -0.13$ and two lower values of e, equal to 0.7 and 0.6. In both cases, the λ line forms a loop beginning at the tricritical point, passing through a maximum at a certain temperature $T_{\max}$ and ending at the upper critical end point, in which two critical liquid phases coexist with a demixed solid phase, $T_{\mathrm{u,cep}}$. The same qualitative results have been found for other values of s between -0.1 and -0.22 and for $e = 0.7$ and 0.6. The mechanism leading to such behavior is the following. The attraction between the like particles is considerably stronger and of longer range than in the case of the unlike particles, and this favors demixing. On the other hand, the ideal contribution to the entropy of mixing $S_m = -kN[x \log x + (1-x)\log(1-x)]$ decreases if phase separation takes place and hence favors mixing. For sufficiently small e and at moderate densities, the attraction between like particles wins over the entropic effects and a phase separation takes place. Upon the increase of density, the attraction between the like particles lowers due to the decrease of average distance between nearest neighbors, while the attraction between the unlike particles increases. This, together with the entropic contributions, leads to the recovery

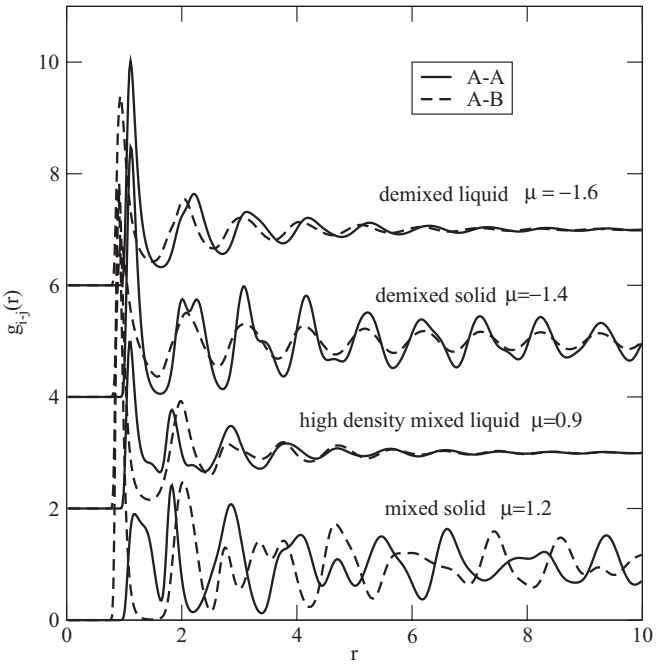

FIG. 12. The radial distribution functions $g_{A-A}(r)$ and $g_{A-B}(r)$ calculated for the system with $s = -0.15$ and $e = 0.6$ at the temperature $T = 0.42$ and for different values of the chemical potential corresponding to the regions of stability of different condensed phases. For clarity, the radial distribution functions for $\mu = 0.9, -1.4$, and -1.6 have been shifted upward by 2, 4, and 6, respectively.

of miscibility. The calculations of radial distribution functions have demonstrated that the high density mixed liquid is locally ordered and exhibits a dominating contribution due to *A*-*B* nearest neighbors. The locations of first maxima at $g_{A-A}(r)$ and $g_{A-B}(r)$ indicate the presence of local square ordering. In Fig. 12, we have given the examples of radial distribution functions calculated for the system with $s = -0.15$ and $e = 0.6$ at $T = 0.42$ and for different values of μ corresponding to the regions of stability of mixed and demixed solid and liquid phases.

Figure 13 gives a sort of a global phase diagram for the systems with $s = -0.13$, which shows the changes in the phase diagram topology upon the variation of the parameter e. In the region of e lower than about 0.735, the phase diagrams are similar to the ones presented in Fig. 11, while for e exceeding 0.735 they are similar to that given in Fig. 10. This is just an example of results. Qualitatively the same behavior have been found for $s = -0.1$ and -0.15.

From the results given in Fig. 13, it follows that the temperature at the lower critical end point, $T_{\mathrm{l,cep}}$, decreases more rapidly than the triple point temperature $T_{\mathrm{tr},v,l_d s_{d,h}}$, when e becomes higher. Therefore, one expects that $T_{\mathrm{l,cep}}$ reaches $T_{\mathrm{tr},v,l_d s_{d,h}}$, when e is high enough. Our data suggest that it should occur when $e \approx 0.86$, so that for still higher values of e the liquid does not phase separate at all.

In the case of systems belonging to region 4 in Fig. 7, the lowering of e also increases the tendency toward demixing in the liquid phase. We have found that when $e = 0.7$ the system with $s = -0.2$ has the phase diagram topology like the systems belonging to region 3 (see Fig. 11), while the system

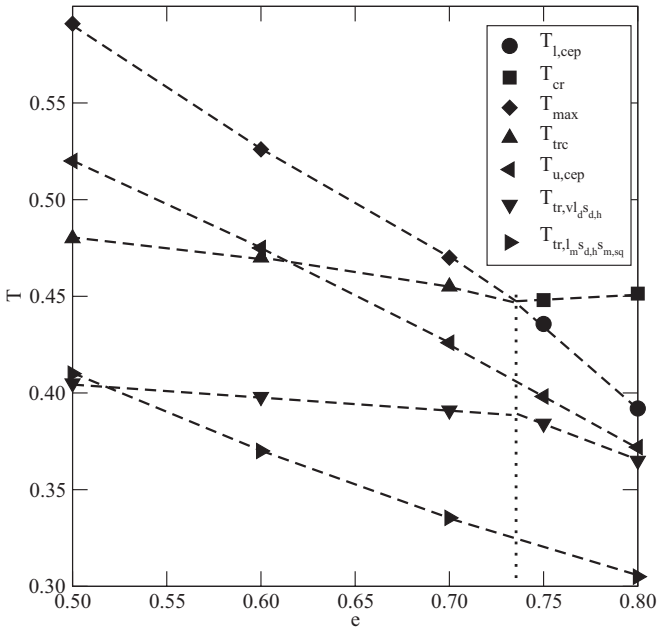

FIG. 13. The changes of the phase diagram topology with e for the systems with $s = -0.13$. The vertical dotted line marks the value of e delimiting the regimes with different phase diagram topology as explained in the text.

with $s = -0.22$ is still qualitatively the same as the phase diagrams shown in Fig. 5. Only a further lowering of e to 0.6 changes the phase diagram topology to that characteristic of region 3.

Similarly, the systems with $s = -0.24$ and different values of e have been found to exhibit phase diagrams of different topology. In the case of $e = 0.8$, we have observed the swan-neck type of phase diagram, and the same has been found for $e = 0.7$. However, when $e = 0.6$, the vapor-liquid condensation has been found to occur over a wide temperature range (see Fig. 14). The liquid is demixed along the

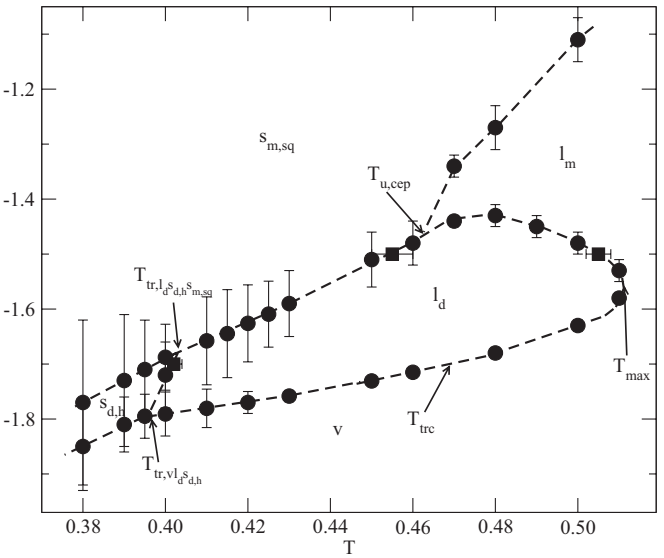

FIG. 14. The $T - \mu$ projection of the phase diagram for the system with $s = -0.24$ and $e = 0.6$.

vapor-liquid coexistence between the triple-point temperature, equal to about 0.396, and the tricritical point, located at the temperature of about 0.47 ± 0.01. At higher temperatures, the demixing transition occurs along the λ line, which shows a closed loop behavior, with $T_{\max} \approx 0.51$, and terminates at the upper critical end point ($T_{\mathrm{u,cep}} \approx 0.462$) at the liquid side of the liquid-(mixed) solid coexistence. At the temperatures below the upper critical end point and above the triple point $T_{\mathrm{tr},s_d,h s_{m,\mathrm{sq}},l_d} \approx 0.402$, the demixed liquid freezes directly into a mixed solid.

IV. SUMMARY AND FINAL REMARKS

We have used Monte Carlo simulations in the grand canonical ensemble to investigate the phase behavior of symmetrical binary mixtures with negative nonadditivity in both the size and the potential well depth. We have studied the evolution of the phase diagram topology when the parameters determining the range (s) and strength (e) of interaction between unlike pairs vary.

It has been demonstrated that when the nonadditivity parameter s is negative and sufficiently low, the demixing transition in the liquid occurs at low densities and then the mixing is recovered at sufficiently high densities. As long as the onset of the demixing transition is at the critical end point below the vapor-liquid critical point, the slope of the λ line with respect to the chemical potential, as well as with respect to the total density, decreases when the parameter s lowers and becomes negative for sufficiently low s. On the other hand, when the interaction between unlike particles is sufficiently weak to drive the onset of the λ line to the tricritical point, the demixing transition in the liquid occurs at the temperatures lower than a certain temperature $T_{\max}$ and only at sufficiently low densities. At high densities, a reentrant mixing occurs.

In general, the lowering of the range of interaction between unlike particles, measured by the parameter s, enhances the tendency toward mixing at high densities and leads to the reentrant mixing in the liquid phase. On the other hand, the lowering of the potential well depth of the interaction between the unlike particles enhances demixing. These two competing effects lead to the closed-loop behavior. In particular, in the systems with sufficiently low e, the λ line starts at the tricritical point and goes up to a certain maximum temperature and then it terminates at the critical end point at the liquid-(mixed) solid coexistence.

It has been also demonstrated that the structure of a mixed solid phase is dominated by the packing effects. When the system exhibits small negative nonadditivity ($s \geqslant -0.1$), the mixed solid has a hexagonal symmetry, just the same as the demixed solid. When, however, the effects of nonadditivity become large enough and s drops below about -0.1, the mixed solid has a square symmetry. These findings agree quite well with the earlier studies of Vlot *et al.* [20].

At this point, we should recall the results obtained by Almarza *et al.* [30] already mentioned in the Introduction. These authors have also obtained a closed-loop fluid-fluid immiscibility in (three-dimensional) symmetrical mixtures. However, they have used the square-well potential and found the closed-loop behavior when the interaction between the unlike particles was of shorter range ($s < 0$) and stronger

($e > 1$) than the interaction between the like pairs. At low densities, a longer range of *A*-*A* than *A*-*B* attractive interaction favors *A*-*A* neighbors and hence leads to demixing. In that regime, the effective *A*-*A* attraction is stronger than *A*-*B* attraction. At high densities, however, the packing effects and strong attraction between *A*-*B* pairs lead to reentrant mixing. We should also mention the recently published results of Amore, Horbach, and Egry [39]. These authors have considered symmetrical binary mixtures with $s = 0$ and Lennard-Jones-like interaction potentials with adjustable attraction term and have demonstrated that in the systems with purely repulsive interactions, demixing occurs only when the repulsion is stronger for *A*-*B* than for *A*-*A* pairs, i.e., when $e > 1$. Of course, in the systems with attraction term "turned-on," the demixing transition occurs only when $e < 1$. Our study has shown that the recovery of miscibility at high densities, in both liquid and solid phases, is driven by packing effects.

[1] J. S. Rowlinson and F. L. Swinton, *Liquids and Liquid Mixtures*, 3rd ed. (Butterworths, London, 1982).
[2] D. Gazzillo, J. Chem. Phys. **95**, 4565 (1991).
[3] J. Jung, M. S. Jhon, and F. R. Ree, J. Chem. Phys. **102**, 1349 (1995).
[4] A. Santos, M. L. de Haro, and S. B. Yuste, J. Chem. Phys. **122**, 024514 (2005).
[5] A. Z. Panagiotopoulos, N. Quirke, M. Stapleton, and D. J. Tildesley, Mol. Phys. **63**, 527 (1988).
[6] C. Caccamo and G. Guinta, Mol. Phys. **78**, 83 (1993).
[7] E. de Miguel, E. M. del Rio, and M. M. Telo da Gama, J. Chem. Phys. **103**, 6188 (1995).
[8] N. B. Wilding, Phys. Rev. Lett. **78**, 1488 (1997).
[9] N. B. Wilding, Phys. Rev. E **55**, 6624 (1997).
[10] N. B. Wilding, F. Schmid, and P. Nielaba, Phys. Rev. E **58**, 2201 (1998).
[11] G. Kahl, E. Schöll-Paschinger, and A. Lang, Monat. Chem. **132**, 1413 (2001).
[12] E. Schöll-Paschinger, D. Levesque, J.-J. Weis, and G. Kahl, Phys. Rev. E **64**, 011502 (2001).
[13] O. Antonevych, F. Forstmann, and E. Diaz-Herrera, Phys. Rev. E **65**, 061504 (2002).
[14] N. B. Wilding, Phys. Rev. E **67**, 052503 (2003).
[15] D. Pini, M. Tau, A. Parola, and L. Reatto, Phys. Rev. E **67**, 046116 (2003).
[16] E. Schöll-Paschinger, E. Gutlederer, and G. Kahl, J. Mol. Liq. **112**, 5 (2004).
[17] D. Woywod and M. Schoen, Phys. Rev. E **73**, 011201 (2006).
[18] J. Köfinger, N. B. Wilding, and G. Kahl, J. Chem. Phys. **125**, 234503 (2006).
[19] N. Dorsaz and G. Foffi, J. Phys.: Condens. Matter **22**, 104113 (2010).
[20] M. J. Vlot and J. P. van der Eerden, J. Chem. Phys. **109**, 6043 (1998).
[21] M. J. Vlot, S. Claasen, H. E. A. Huitema, and J. P. van der Eerden, Mol. Phys. **91**, 19 (1997).
[22] S. Sengupta, D. Marx, P. Nielaba, and K. Binder, Phys. Rev. E **49**, 1468 (1994).
[23] S. K. Das, J. Horbach, K. Binder, M. E. Fisher, and J.-V. Sengers, J. Chem. Phys. **125**, 024506 (2006).
[24] A. Patrykiejew and S. Sokołowski, Phys. Rev. E **81**, 012501 (2010).
[25] S. Materniak, A. Patrykiejew, and S. Sokołowski, J. Chem. Phys. **133**, 244501 (2010).
[26] J. Hirschfelder, D. Stevenson, and H. Eyring, J. Chem. Phys. **5**, 896 (1937).
[27] J. A. Barker and W. Fock, Discuss. Faraday Soc. **15**, 188 (1953).
[28] T. Narayanan and A. Kumar, Phys. Rep. **149**, 135 (1994).
[29] J. N. C. Lopes, Molec. Phys. **96**, 1649 (1999).
[30] N. G. Almarza, E. Enciso, M. F. García, M. A. González, and F. J. Bermejo, Phys. Rev. E **64**, 012501 (2001).
[31] P. H. van Konynenburg, and R. L. Scott, Philos. Trans. Roy. Soc A **298**, 495 (1980).
[32] J. A. Barker and D. Henderson, Rev. Mod. Phys. **48**, 587 (1976).
[33] D. A. Kofke and E. D. Glandt, Molec. Phys. **64**, 1105 (1988).
[34] D. Frenkel and B. Smit, *Understanding Molecular Simulation: From Algorithms to Applications* (Academic Press, San Diego, 1996).
[35] M. P. Allen and D. J. Tildesley, *Computer Simulation of Liquids* (Oxford University Press, Oxford, 1987).
[36] D. P. Landau and K. Binder, *A Guide to Monte Carlo Simulation in Statistical Physics* (Cambridge University Press, Cambridge, 2000).
[37] M. J. Vlot and H. E. A. Huitema, A de Vooys, and J. P. van der Eerden, J. Chem. Phys. **107**, 4345 (1997).
[38] M. J. Vlot, J. Cornelis van Miltenburg, H. J. A. Oonk, and J. P. van der Eerden, J. Chem. Phys. **107**, 10102 (1997).
[39] S. Amore, J. Horbach, and I. Egry, J. Chem. Phys. **134**, 044515 (2011).